Rapid transition from High-Pressure metamorphism to orogen-parallel exhumation driven by extensional shearing (Adula unit, eastern Central Alps)

C. Montemagni[1], R. Monti[2], N. Malaspina[2], P. Vannucchi[1] and S. Zanchetta[2]

[1]Department of Earth Sciences, University of Florence, Via la Pira 4, 50121, Firenze, Italy.

[2]Department of Earth and Environmental Sciences, University of Milano Bicocca, Piazza della Scienza 4, 20126 Milano, Italy.

Corresponding author: Chiara Montemagni (chiara.montemagni@unifi.it)

Key Points:

- First dated Alpine eclogites in the northern Adula nappe by means of $^{40}Ar/^{39}Ar$ geochronology extend Alpine HP metamorphism northward
- Peak Alpine HP metamorphism recorded at 38-39 Ma at P-T of 2.0-2.4 GPa and 580-655 °C
- Rapid switch from nappe stacking to extensional shearing within ~5 Myrs

Abstract

In the Central Alps, the Adula unit exposes high- and ultra-high-pressure (HP-UHP) metamorphic rocks, providing key insights into the subduction and exhumation dynamics of the former distal European margin. We investigate the San Bernardino Shear Zone (SBSZ), a top-to-the-east extensional shear zone developed within orthogneiss and paragneiss at the top of the Adula unit, containing eclogite boudins. Using detailed structural analysis, petrography, thermodynamic modelling, and $^{40}Ar/^{39}Ar$ geochronology, we constrain the Pressure-Temperature-deformation-time (P-T-d-t) path of these HP rocks.

Phengite in eclogites yields peak metamorphic ages of 38-39 Ma, making them the northernmost Alpine HP record in the Adula nappe. Eclogite facies conditions reached ~2.0-2.4 GPa and 580-655 °C. Progressive deformation led to the overprinting of earlier NW-directed fabrics by top-to-the-east shearing, recorded in synkinematic mica and associated with resetting of $^{40}Ar/^{39}Ar$ ages to 36-29 Ma. This temporal-spatial pattern indicates a short interval between subduction, nappe stacking, and extensional exhumation.

Our results demonstrate that the SBSZ played a key role in the exhumation of the eastern Lepontine Dome, supporting a model of distributed orogen-parallel extension. This mechanism, partially coeval with amphibolite-facies metamorphism and crustal anatexis, suggests that HP units were exhumed during orogen-perpendicular shortening and orogen-parallel extension.

1 Introduction

The exhumation of high-pressure (HP) and ultra-high-pressure (UHP) metamorphic rocks in collisional belts has been a central topic of tectonic research for decades, yet significant debate remains over the geometry and driving mechanisms behind these processes (see Hacker & Gerya, 2013 for further discussion). One ongoing issue is the extent of tectonic re-organization observed in HP units. Some works (e.g. Trommsdorff, 1990; Engi et al., 2001) argue that what appear to be coherent HP units are actually tectonic mélanges, where fragments of various origins have mixed along the plate interface during the subduction–exhumation cycle. These fragments might represent small blocks with distinct Pressure-Temperature-deformation-time (P-T-d-t) paths, possibly experiencing multiple cycles of subduction and exhumation over a few million years (e.g., Gerya et al., 2002; Rubatto et al., 2011). This hypothesis, primarily supported by numerical models, suggests that material returns via low-density channels, a concept largely based on petrologic and geochemical data (Federico et al., 2007; Sandmann et al., 2014).

Chaotic mixing models have become increasingly popular for oceanic HP units (e.g., Gerya et al., 2002; Federico et al., 2007; Vannucchi et al., 2012), which commonly contain serpentinite-dominated matrix incorporating fragments of continental and oceanic crust and mechanically weak structures. For continental HP units instead, the relevance of subduction-channel mélange models is more uncertain, with some Authors (e.g., Chemenda et al., 1995; Nagel, 2008) suggesting that entire coherent (U)HP units are exhumed during single events.

The Adula unit in the Lepontine Dome of the eastern central Alps (Figure 1) is one of the classical areas of the Alps where (U)HP eclogite-facies metamorphism occurred (e.g., Nagel, 2008). This unit consists of various gneisses with calcschists, marbles and the local occurrences of eclogites and garnet peridotites in the Cima Lunga subunit (Heinrich, 1986).

The Adula unit was suggested to be a chaotic subduction channel mélange (Trommsdorff, 1990), with some studies concluding that it consists of rocks from different palaeogeographic origins and/or distinct subduction histories (e.g., Trommsdorff, 1990; Engi et al., 2001; Berger et al., 2005), possibly already formed as a melange during the Variscan orogeny (Tagliaferri et al., 2023). Other researches, however, suggests it represents a relatively coherent basement unit, at least since peak-pressure conditions during the Alpine event (e.g., Dale & Holland, 2003; Nagel, 2008; Herwartz et al., 2011; Cavargna-Sani et al., 2014; Ring & Glodny, 2021).

In this context, it is critical to unravel the exhumation processes of HP rocks in the Lepontine Dome, and therefore essential to perform comprehensive field investigations, along with structural, petrological, and geochronological studies of these HP rocks.

The exhumation of HP units can occur by different mechanisms, among which some implying transient extension within the evolving orogenic wedge (e.g. Beltrando et al., 2010; Malusà et al., 2015). The modes of exhumation have a significant impact on the retrograde P-T paths after the pressure peak: steep geothermal gradients that allow a cold exhumation of eclogites or regional Barrovian overprint of the HP rocks (Beltrando et al., 2010) in a very short time after the pressure peak. The second case best fits the tectono-metamorphic history of the Adula unit. Indeed, Adula is part of a crustal nappe stack made of tectonic units derived from the distal margin of the European plate, the Mesozoic basins and the Briançonnais microcontinent (Stampfli et al., 1998; Handy et al., 2010). These units were stacked together northward (e.g. Nagel et al., 2008) and later up-arched to form the Lepontine Dome during the late Eocene-Oligocene continent-continent collision (e.g. Merle & Guillier, 1989; Schmid et al., 1996; Wiederkher et al., 2009, Steck et al., 2013). The up-doming of the Lepontine Dome was accommodated by several crustal-scale shear zones at its boundary. To the West, the extensional Simplon Fault (Figure 1a; e.g. Mancktelow, 1985) promoted the exhumation of the western part of the Dome (the Toce culmination) between 20 and 8 Ma (see Montemagni & Zanchetta, 2022 and Wolff et al., 2024 for updated reviews). To the East (the Ticino culmination), no prominent structures such as the Simplon Fault occur, but a series of post metamorphic minor extensional faults (Figure 1a; Rahn, 2005; Tagliaferri et al., 2023) between the Europe-derived units or in the Austroalpine (i.e. Africa derived tectonic units) in the hanging-wall of the Dome (Ring & Glodny, 2021).

However, extensional shearing at the top of the eastern termination of the Lepontine Dome is not only confined in the hanging-wall Austroalpine units, but significant crustal extension has been likely accommodated also within the Adula nappe. In the San Bernardino Pass area (Figure 1b) in South Switzerland we identified a shear zone (the San Bernardino Shear Zone, SBSZ) developed within orthogneiss and eclogite-bearing paragneiss layers at the top of the Adula nappe. By means of detailed geological mapping, meso- and micro-structural analysis, petrography, geothermobarometry and $^{40}Ar/^{39}Ar$ dating, we reconstructed the P-T-d-t (Pressure-Temperature-deformation-time) paths of the eclogites and the hosting rocks. The San Bernardino eclogites, dated for the first time, resulted to be the northernmost HP rocks of Alpine age in the Adula nappe. The occurrence of eclogites within the SBSZ allowed us to have a complete view from the Alpine HP stage to the exhumation of eclogites passing through the regional Barrovian overprint. The wealth of data helped to pinpoint the role of this extensional shear zone in the exhumation of the (U)HP Adula unit and the eastern part of the Lepontine Dome.

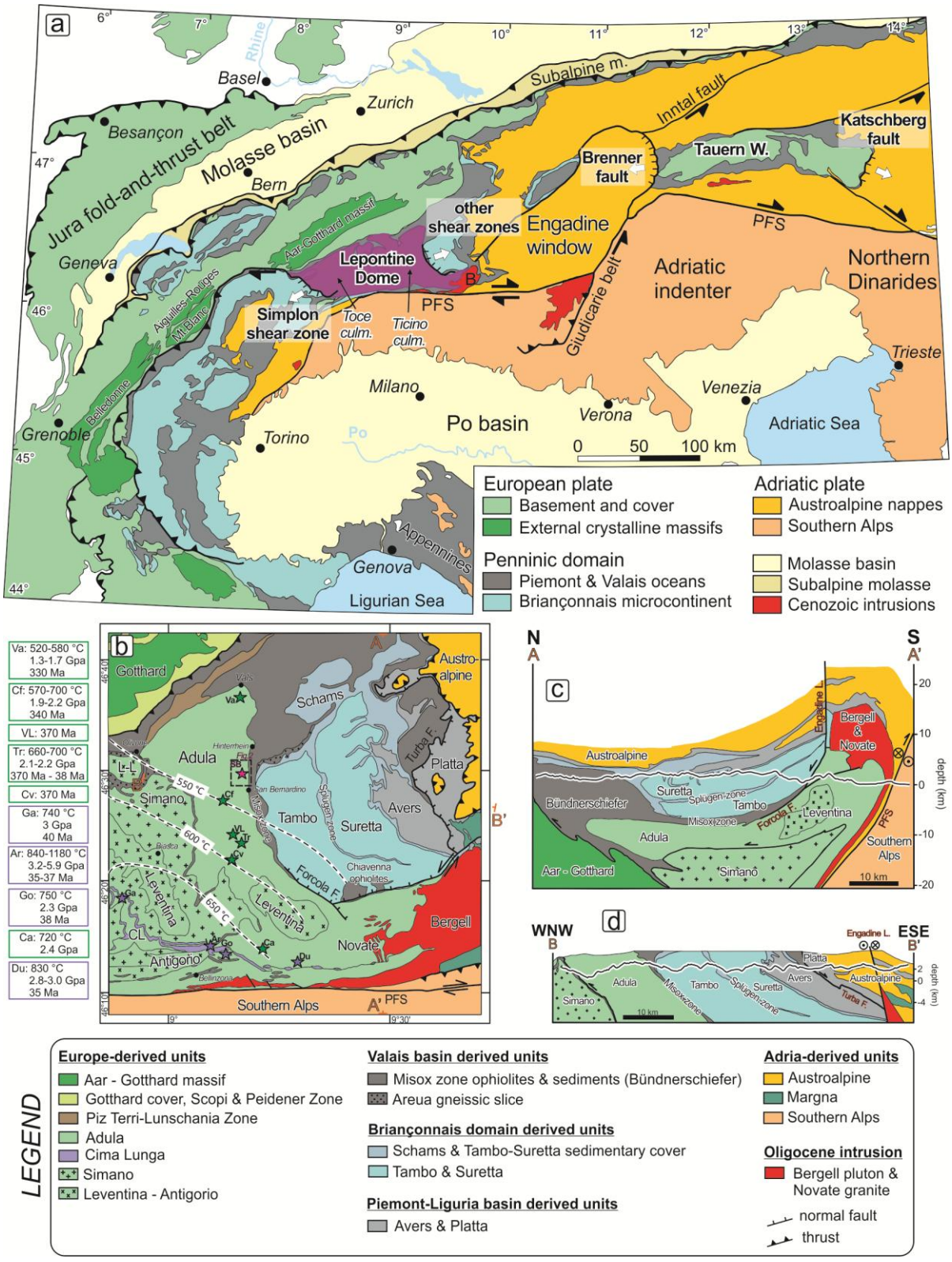

Figure 1. (a) Simplified geological map of the European Alps (after Schmid et al., 2004; Handy et al., 2010), in which the Lepontine Dome has been highlighted together with the extensional structures at its eastern and western borders. (b) Tectonic map of the Lepontine nappe stack (after Pleuger et al., 2008 and Herwartz et al., 2011) with reported isotherms for the post nappe-stacking Barrovian metamorphic event crosscutting nappe boundaries (from Todd and Engi, 1997). Rectangle shows the position of the map reported in Fig. 2. Eclogite or garnet bearing

peridotite localities have been shown with green (Adula Unit) or violet (Cima-Lunga Unit) stars. Boxes illustrate a compilation of peak PT and high-pressure ages (Liati et al., 2009, Herwartz et al., 2011). CL Cima Lunga Unit, L-L Lucomagno-Leventina Unit. Va, Vals; Cf, Confin; VL, Val Large; Tr, Trescolmen; Cv, Calvaresc; Ga, Gagnone; Ar, Alpe Arami; Go, Gorduno; Ca, Caurit; Du, Duria). (c) and (d) Simplified cross sections (after Ring and Glodny, 2021). (c) N-S (A-A') perpendicular to the regional Alpine strike showing the sequence of crystalline nappes (Adula, Tambo and Suretta) and interlayered sediment zones, and their structural relationship to the Bergell intrusion. (d) WNW-ESE cross section B-B'.

2 Geological Background

The Central Alps started to form in the middle Eocene in response of the closure of the Mesozoic Alpine Tethys and the collision between the southern European and northern Adriatic margins (e.g. Handy et al., 2010; Stampfli et al., 1998). The continent-continent collision took place in the late Eocene – early Oligocene following the subduction beneath northern Adria of the oceanic lithosphere and related sediments of the Alpine Tethys oceanic basin, as well as part of the European continental crust (Gebauer, 1996; Schmid et al., 1996; Wiederkehr e al., 2009).

As a consequence of collision, the European basement nappe were thrust northward between 33 and 36 Ma forming the Penninic nappe-stack of the Central Alps (Nagel et al., 2002; Rahn, 2005; Nagel, 2008; Wiederkehr e al., 2008, 2009; Steck et al., 2013; Cavargna-Sani et al., 2014; Kossak-Glowczewski et al., 2017). After or during nappe stacking (see Tagliaferri et al., 2023 for discussion) a Barrovian metamorphism interested all the Penninic tectono-metamorphic units forming the Lepontine Dome, with concentric isotherms that crosscut nappe boundaries (Figure 1b). Temperature increases southward, reaching a maximum within the Southern Steep Belt (Figure 1b), close to the Periadriatic Fault, where diffuse migmatisation occurred (e.g. Burri et al., 2005).

The tectono-metamorphic units of the Lepontine Dome derive from the hyperextended European margin and from the Alpine Tethys and the Briançonnais microcontinent (Schmid et al., 2004) that separated the Alpine Tethys Ocean in two basins (N and S Penninic oceans, Handy et al., 2010). The several units experienced heterogeneous P-T paths before the nappe-stacking phase and the formation of the Lepontine Dome (e.g. Tagliaferri et al., 2023).

The Adula unit, together with Simano e Lucomagno-Leventina units, belongs to the Lower Penninic nappe complex derived from the distal European margin of the Helvetic domain. At present Adula unit lies below the Tambo and Suretta Middle Penninic nappes derived from the Briançonnais domain, which originally formed a horst structure between a marginal ocean basin (Valaisan trough) to the N and an open ocean to the S (Figure 1b; e.g. Gebauer, 1996; Pleuger et al., 2003; Nagel et al., 2002; Schmid et al., 2004; Nagel, 2008; Wiederkehr et al., 2009; Steck et al., 2013; Cavargna Sani et al., 2014; Steck et al., 2019). According to palaeogeographical reconstructions (Schmid et al., 2004), the original position of the Adula nappe is at the former distal European margin, facing the Valais Ocean, which opened in the Late Jurassic and closed during the Late Cretaceous–Eocene convergence between Europe and Africa–Adria (Dewey et al., 1989).

At the base the Adula unit is in contact with the Simano Unit. If the contact is not occurring along the Mesozoic metasedimentary cover of the Simano nappe, then it is not always well

distinguishable, due to the similarity between the Simano basement gneiss, and the overprinting caused by the Barrovian late Cenozoic metamorphism.

At the top, the Adula unit is separated from the Middle Penninic units by the Misox zone (Mesolcina zone of Cavargna Sani et al., 2014), a thin unit of mainly Valaisan (North Penninic) provenance (e.g. Schmid et al. 1996) composed by several slices of metasedimentary clastic rocks (the "North Penninic Bündnerschiefer", Pleuger et al., 2003), MORB-derived amphibolites and slices of continental basement.

The Adula unit is primarily composed of orthogneiss and paragneiss. The magmatic protoliths of the orthogneiss have Ordovician or Early Permian intrusion ages (Steck et al., 2013; Cavargna-Sani et al., 2014). The paragneisses are frequently interleaved with amphibolites and metacarbonates. Amphibolites often preserve eclogitic relicts and well-preserved eclogite boudins are preserved in several localities (Brouwer et al., 2005 with references). Slices of the metamorphosed Adula Mesosozic sedimentary cover are mainly preserved in the norther part of the unit (Galster et al., 2012; Cavargna-Sani et al., 2014).

During the Eocene-Oligocene Alpine orogenic cycle, the Adula nappe, along with the crustal fragments which now form the Southern Steep Belt, was subducted to mantle depths (Evans & Trommsdorff, 1978; Heinrich, 1986; Becker, 1993; Gebauer, 1996). Metamorphic conditions at peak pressure decrease northward, from 2.5–3.0 GPa and ca. 750 °C in the south to 2.2 GPa and 750 °C in the middle to 1.7 GPa and 640 °C in the north (Dale & Holland, 2003; Brouwer et al., 2005). Rocks of the Adula unit experienced HP metamorphism also during the Variscan orogeny. Eclogitic relicts dated to 330-370 Ma are preserved in the northern part of the unit (Liati et al., 2009), whereas eclogites of the southern Adula have an Alpine age (35-47 Ma, Becker, 1993; Liati et al., 2009; Brouwer et al., 2005; Sandmann et al., 2011). In the middle part of the nappe both Variscan and Alpine ages occur (Trescolmen eclogites, Herwartz et al., 2011).

3 The San Bernardino Shear Zone

The SBSZ is up to ca. 500 m-thick, top-to-the-E extensional shear zone atop the Adula unit (Figure 2) developed in orthogneiss and paragneiss containing eclogite boudins. The mylonitic foliation (S_2) dips to the E (Figure 2) with an NW-SE trending L_2 lineation (Figure 2b) mainly developed within orthogneisses. The D_2 L-S fabric, pervasive all over the investigated area, is associated to a top-to-NW sense of shear, defined on the base of kinematic indicators developed both at the meso (s and d clasts, SCC' structures) and at the microscale.

From the San Bernardino Pass area looking towards the E the NE-dipping foliation of the Adula unit is clearly observable, together with the Misox and Tambo units above. Eclogite boudins (Figure 2c) are hosted in paragneiss levels that occur close to the Adula-Misox boundary. Boudins range from a few meters to several hundred of meters in size (Figure 2). They almost invariably display a mylonitic foliation (S_1 in Figure 2b) and lineation (L_1) marked by the Shape Preferred Orientation (SPO) of white mica, clinopyroxene and quartz rods (Figure 2d-e). Up to 3 mm in size prismatic porphyroblasts of blue amphibole occur in several outcrops. Amphiboles are weakly to strongly iso-oriented with the eclogitic lineation (Figure 2e), suggesting they crystallized during the late stages of the eclogitic D_1 deformation event. Eclogitic boudins are flattened along the S_2 mylonitic foliation developed in orthogneiss and paragneiss. The eclogitic L_1 lineation appears to

be randomly oriented, suggesting a relative rotation with respect to the dominant L_2 mylonitic lineation developed in the host rock (Figure 2b).

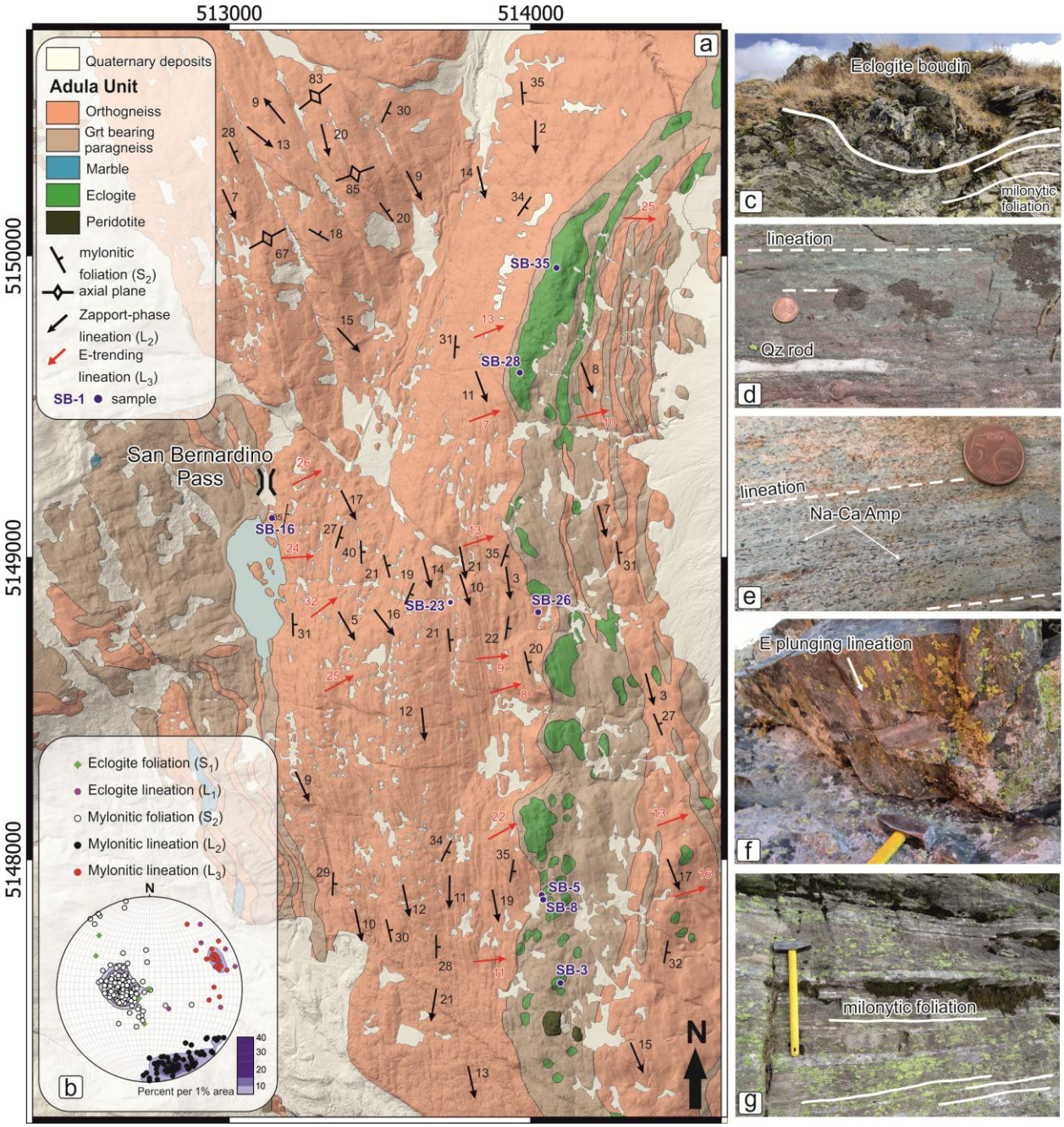

Figure 2. (a) Geological maps of the San Bernardino Pass area, WGS84 UTM 32N. (b) Equal area, lower hemisphere stereographic projections of foliation (S_1) and lineation (L_1) in eclogite boudins and, mylonitic foliation (S_2) and lineation referred to the Zapport phase (L_2) and to the orogen parallel extension phase (L_3). (c) Eclogite boudin hosted in paragneiss. (d) Eclogite lineation on foliation plane highlighted by Qz rods and (e) by Na-Ca amphibole. (f) ENE-plunging lineation becoming predominant close to the Misox zone. (g) Orthogneiss E-dipping mylonitic foliation.

The D_2 mylonitic fabric is overprinted by a younger mylonitic lineation (L_3) developed along the S_2 foliation planes, but oriented at high angle (Figure 2a-2b) with respect to L_1. L_3 is associated to a top-to-E sense of shear, mainly defined from microstructural observations on oriented thin sections (see Section 5), as kinematic indicators at the mesoscale appear to be poorly developed. The ENE to WSW-trending L_3 becomes increasingly pronounced from the bottom (W) to the top (E) of the shear zone itself. L_3 is chiefly developed within orthogneiss or at the rims of the eclogitic boudins (Figure 2f), likely as a consequence of the rheological contrast between eclogite and the host paragneiss. For samples location see Table S1.

4 Analytical methods

The details of the analytical procedures (i.e. EMPA, $^{40}Ar/^{39}Ar$ dating, thermodynamic modelling etc.) are described in the following section. Mineral name abbreviations are explained in the caption of **Figure 3**.

4.1 Electron Probe Micro Analysis

Mineral compositions were measured with the JEOL 8200 Super Probe EMP at the Department of Earth Sciences Ardito Desio, University of Milano. The analysis was carried out using five wavelength dispersive spectrometers with an accelerating voltage of 15 kV, a beam current of 5 nA with a spot size of 3 µm on micas and 1 µm on other minerals. Natural silicates and oxides were used as standards. Analyses were recalculated to atom per formula unit (a.p.f.u.) as follows: white mica analyses were elaborated based on 11 oxygens and considering all Fe as Fe^{2+}; garnet was recalculated based on 8 cations and 24 charges; clinopyroxene analyses were recalculated following the procedure by Cawthorn and Collerson (1974) based on 12 oxygens and considering Fe^{3+} as the acmite component; amphiboles analyses were recalculated based on 23 oxygens and 13 cations plus K, Na, Ca. Amphiboles were classified according to Hawthorne and Oberti (2007). In all tables, the abbreviations are after Whitney and Evans (2010) except for white mica (Wm).

4.2 $^{40}Ar/^{39}Ar$ dating

Samples selected for $^{40}Ar/^{39}Ar$ dating were crushed and sieved in order to separate phengitic white mica (in the fraction 125-250 and 250-500 µm to exclude the hypothesis of Ar diffusion and Ar excess, Villa et al., 2014) from orthogneiss and eclogite for stepwise heating experiments. The separates were enriched in white mica by prolonged handpicking under a stereomicroscope. Mineral separates were then cleaned ultrasonically in deionized water and wrapped in aluminum foil. Samples and standards were irradiated for 10 MWh in a fast neutron flux at the McMaster University Research Reactor (Hamilton, CA). Stepwise heating experiments were performed at the 'Laboratorio di Geocronologia' of the University of Milano–Bicocca following the procedure reported in Montemagni and Villa (2021) and Montemagni and Zanchetta (2022). Sample and standards were loaded in a double vacuum resistance furnace attached to a NuInstruments™ Noblesse® noble gas mass spectrometer, equipped with one Faraday collector with a 1011Ω resistor and two MasCom™ ion counters. The samples were heated in 8-10 steps for 20 min each. The irradiation intensity factor, J, was interpolated for each sample from the equation defined by the J values of the monitors. The ^{40}K decay constant used for the age calculation was 5.543×10^{-4} Ma^{-1} reported in Steiger and Jäger (1977). The vertical flux gradient has been controlled by

monitors of McClure Mountain hornblende (MMhb) which were interlayered with the sample disk wraps. The age of MMhb has been reported in Schoene and Bowring (2006) to be 523.98 ± 0.12 Ma.

4.3 Thermodynamic modelling and geothermobarometry

Thermodynamic modelling was performed in the MnO-Na_2O-CaO-K_2O-FeO-MgO-Al_2O_3-SiO_2-H_2O-TiO_2-O (MnNCKFMASTO) system with the software package GeoPS (http://www.geops.org; Xiang & Connolly, 2022), using the revised version (2004, hp04ver.dat) of the thermodynamic database of Holland and Powell (1998). A carbonate-free eclogite sample was used to derive the chemical composition used for modelling. Sample (SB5, see **Table S1** for sample location) was analyzed by Inductively Coupled Plasma Mass Spectrometry (ICP-MS) for major elements cat the ACME analytical laboratories (Vancouver, Canada) after fusion with lithium metaborate/tetraborate and digestion by diluted HNO_3. Loss on ignition (LOI) was determined by weight difference after ignition at 1000 °C. Blank analyses were always below the minimum detection limit for each element, and the analytical protocol included the analysis of the reference materials (standards) OREAS184, SO-19, OREAS30A and OREAS262. The composition used is the following: SiO_2 (48.46 %), Al_2O_3 (17.12 %), FeO (12.41 %), MgO (6.09 %), Na_2O (3.94 %), K_2O (1.13 %), TiO_2 (2.11 %), MnO (0.22 %). The equation of state for a binary fluid H_2O-CO_2 of Holland and Powell (1998) was adopted, considering fluid saturated conditions with a pure H_2O fluid.

The used A-X solutions are from White and Powell (2002) (WPC), Holland and Powell (2011) (HP11), White et al. (2014) (W), Green et al. (2016) (G): Chl(W) for chlorite, Gt(W) for garnet, Mica(W) for muscovite-paragonite, Crd(W) for cordierite, Bi(W) for biotite, Ctd(W) for chloritoid, St(W) for staurolite, melt(G) for melt, FSP(WPC) for ternary feldspar, Ilm(W) for ilmenite, Opx(W) for orthopyroxene, Omph(G) for omphacite, cAmph(G) for amphibole, EP(H11) for epidote. Pure phases considered in modelling include quartz/coesite, rutile, titanite, lawsonite and H_2O. The results of forward thermodynamic modelling have been compared with conventional geothermobarometry. The phase equilibrium assemblage of the San Bernardino eclogites (Grt + Cpx + Ph ± Ky) responds to the conditions requested by the geothermometer of Krogh Ravna (2000) and the geothermobarometer of Krogh Ravna and Terry (2004). P-T estimates were obtained for three eclogite samples (SB3, SB5 and SB35, see **Table S1** for sample details). Cpx – Grt – Ph in textural equilibrium and directly in contact to each other were selected and their composition estimated by EPMA analysis.

5 Petrochronology

5.1 Microstructures and mineral chemistry

5.1.1. Eclogites

Two types of eclogites crop out within the SBZS: carbonate-free (type 1) and carbonate-bearing (type 2). We focused our attention on type 1 eclogites as they are by far the most abundant and, thanks to their simpler mineralogy, they are more suitable for thermodynamic modelling. Type 1 eclogites mineralogy is made of garnet, clinopyroxene, white mica, amphibole, rutile, quartz, and clinozoisite. Apatite, zircon and ilmenite occur as accessory phases. The mean grain size ranges

from <50 µm up to 250 µm for garnet porphyroblasts, 50-350 µm for clinopyroxene and white mica, <100 µm for rutile and up to 2000 µm for amphiboles porphyroblasts grown on the eclogitic foliation (S_1, Figure 2e and Figure 3).

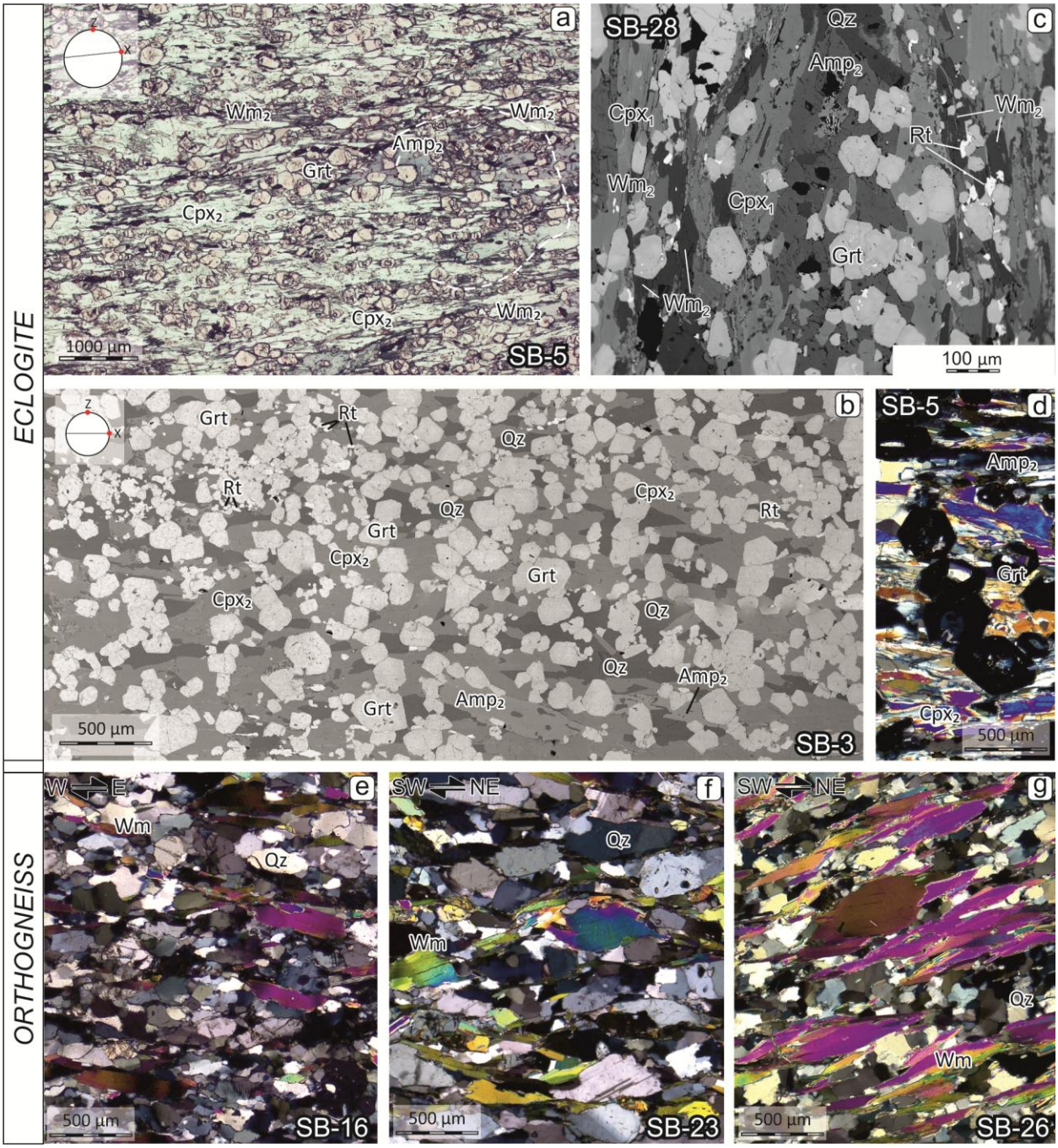

Figure 3. Photomicrographs of San Bernardino eclogites and orthogneisses. (a) Eclogite sample showing the main foliation made of Cpx_1, Amp_2 and Wm_2 surrounding Grt porphyroblasts (parallel polars). (b) BSE panorama of eclogite characterized by a main foliation of Cpx_1, Amp_2 and Wm_2. (c) BSE image of a large Amp2 porphyroblasts syn-kinematic to the eclogitic foliation. Garnet porphyroblasts, when having an aspect ration that differs from 1:1, also appear elongated along the foliation. (d) Cross-polars photo of garnet porphyroblasts within the eclogite, containing inclusions of Wm and Amp. (e), (f) and (g) orthogneiss samples dated by $^{40}Ar/^{39}Ar$ method from bottom to top of the SBSZ. In (e) the older foliation is still evident, whereas is fully overprinted in (g). The mineral abbreviations are as

follows: Amp: amphibole; Ap: apatite; Bt: biotite; Cal: calcite; Chl: chlorite; Cpx: clinopyroxene; Czo: clinozoisite; Dol: dolomite; Grt: garnet; Ilm: ilmenite; Kfs: K-feldspar; Qz: quartz; Pg: paragonite; Pl: plagioclase; Rt: rutile; Ttn: titanite; Wm: white mica; Zr: zircon.

Garnet porphyroblasts elongated parallel to the eclogitic foliation appear optically zoned, with inclusion-rich cores and clean rims (Figure 3a). Garnet inclusions consist of blue amphibole (Amp_1), white mica (Wm_1), quartz and rare rutile (Rt_1). The pre-eclogitic equilibrium phase assemblage preserved in garnet cores is:

$Grt_1 + Amp_1 + Wm_1 + Rt_1 + Qz$

Garnet rims appear to have grown synkinematically to the S_1 eclogitic foliation, as shown by their slightly elongated idiomorphic habit (Figure 3a and Figure 4). S_1 is marked by the SPO of Cpx_1 and Wm_2. Rutile grains (Rt_2) with an elongated habit (aspect ratio 1:2 to 1:3, Figure 3a) are also parallel to S_1. In some samples also porphyroblasts of clinozoisite (Czo_1) up to 800-1000 µm occur. The syn-S_1 eclogitic phase assemblage is:

$Grt_2 + Cpx_1 + Wm_2 + Rt_2 + Qz \pm Czo_1$

In a few samples atoll garnet porphyroblasts occur. Radial fractures crosscutting garnet rims and the occurrence of lobate edges, peninsular structures and ameboid relicts at cores suggests that fluid-assisted resorption ad recrystallization occurred (e.g. Faryad et al., 2010). At the core of atoll garnets there are Qz + Cpx + Wm inclusions that display the same composition of minerals along the S_1 eclogitic foliation. Large (up to 2000 µm, Figure 2e and 3c) blue-colored amphibole porphyroblasts (Amp_2) grow late- to post-kinematic with respect to the S_1 foliation. The HP phase assemblage in eclogites is generally well preserved, with only minor retrogression resulting in symplectites made of $Amp_3 + Cpx_2 + Pl + Qz$ that develop along grain boundaries of Cpx_1 and between Cpx_1 and garnet porphyroblasts.

Type 2 eclogites contain carbonates and paragonitic white mica. Garnet cores of type 2 eclogites have inclusions of Wm_1, Amp_1, Mgs and Qz. White mica (Wm_1) included in garnet cores ha a phengitic composition whereas Wm_2 along foliation is a nearly pure paragonite. The syn-S_1 phase assemblage ($Grt_2 + Cpx_2 + Wm_2 + Rt + Qz + Dol$) is similar to that of type 1 eclogites, except for the occurrence of dolomite porphyroblasts elongated parallel to S_1. Rare calcite crystals also occur.

Cpx_1 in type 1 eclogite has an omphacitic composition, with Jd_{50-57} and *X*Mg (Fe^{2+}) of 0.70-0.80 (**Table S2**). Cpx_2 rarely occurs within symplectites after Cpx_1, together with Amp_3 and Pl. The Na content of Cpx_2 is slightly lower (Jd_{41-48}) than in Cpx_1 (Figure 4c).

Garnet porphyroblasts are compositionally zoned, with decreasing Fe, increasing Mg and almost homogeneous Ca contents from core to rim (Figure 4e-f). The composition of the inclusion-rich core (Grt_1) is $Alm_{55-62}Pyr_{13-21}Grs_{21-24}Sps_{1-2}$ (**Table S3**). Garnet rims (Grt_2) are mainly inclusion-free and formed around Grt_1 cores varying in thickness from 1/10 to 1/3 of the entire porphyroblast diameter (Figure 4e). The representative composition of Grt_2 in type 1 eclogites is $Alm_{50-55}Pyr_{20-30}Grs_{18-22}Sps_{0-2}$ (**Table S3**).

The two white mica generations of type 1 eclogites have phengitic compositions with a little paragonitic component (up to 0.20 Na a.p.f.u.). Wm_1 (included in garnet) and Wm_2 (syn-

kinematic along the S_1 eclogitic foliation) display overlapping Si contents, with Wm_1 ranging from 3.30 to 3.38 a.p.f.u. and Wm_2 that displays a wider range of 3.26-3.39 with decreasing Si from core to rim, especially for samples SB3 and SB35 (Figure 4a**, Table S4**).

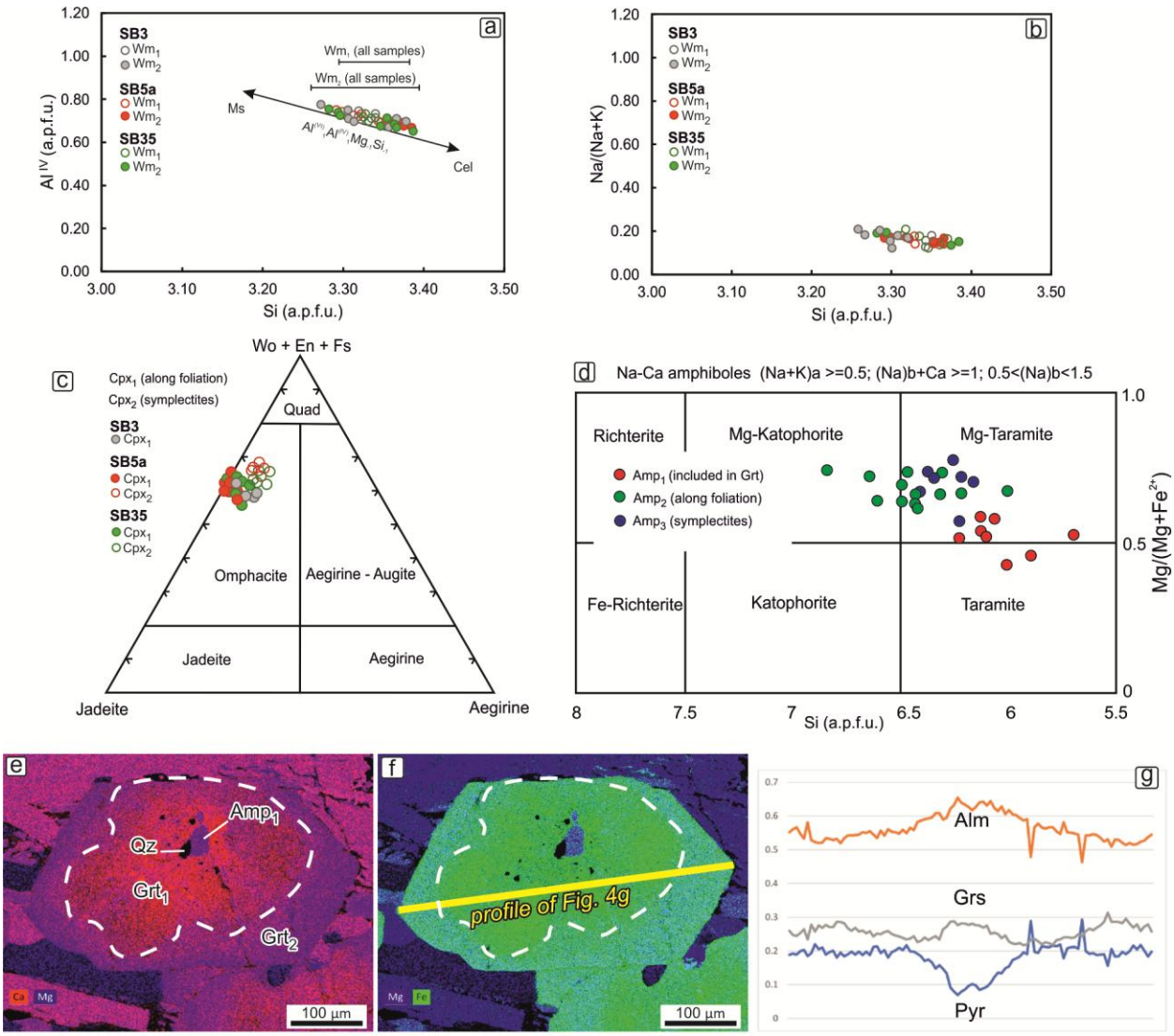

Figure 4. EPMA (Electron Probe Micro Analysis) results showing compositional variation in (a-b) white mica, (c) clinopyroxene, (d) amphibole and (e-g) garnet in eclogite samples.

Both Amp_1 inclusions in garnet cores and Amp_2 porphyroblasts that formed late- to post-kinematic with respect to the S_1 eclogitic foliation, are Na-Ca amphiboles. Amp_1 is a Mg-Taramite, with a Si content around 6 a.p.f.u. and *X*Mg of 0.4-0.6 (Figure 4d). Amp_2 has both higher Si (ca. 6.5 a.p.f.u.) and *X*Mg (0.65-0.70) with respect to Amp_1 (Figure 4d). The M4 site occupancy by Na is 0.5-0.7 for Amp_1 and 0.9-1.1 for Amp_2 (**Table S5**).

5.1.2. Orthogneisses

Within the orthogneiss, from bottom to top of the SBSZ (Figure 3e-g), the S_2, Zapport-phase – the dominant metamorphic event recognized in the Adula nappe associated to top-to-N-NW nappe

stacking and dated around 36-33 Ma (Pleuger et al., 2003) - related, foliation is gradually overprinted (Figure 3f-g) by a younger, sub-parallel, foliation-oriented NNW-SSE and dipping towards the E. This younger foliation is expressed at the microscale by the recrystallization of finer flakes of white mica that envelop older mica fish (Figure 3f-g) and become more pronounced toward the top of the SBSZ (Figure 3g). Quartz recrystallization mechanisms are expressed by Grain Boundary Migration (GBM, Passchier and Trouw, 2005) and window and pinning structures in the structurally lowest samples (Figure 3e), and by Bulging (BLG, Passchier and Trouw, 2005) moving structurally upwards (Figure 3f-g), coherent with a decreasing temperature during top-to-E driven syn-shearing exhumation.

The composition of white mica marking the mylonitic foliation displays a compositional gradient from the bottom to the top of the shear zone. White micas in samples at the bottom (SB16, see Figure 2) have a higher Si content (3.31-3.43 a.p.f.u.) with respect to mylonitic orthogneisses at the top (3.14-3.19 a.p.f.u.), coherent with progressive recrystallization during exhumation.

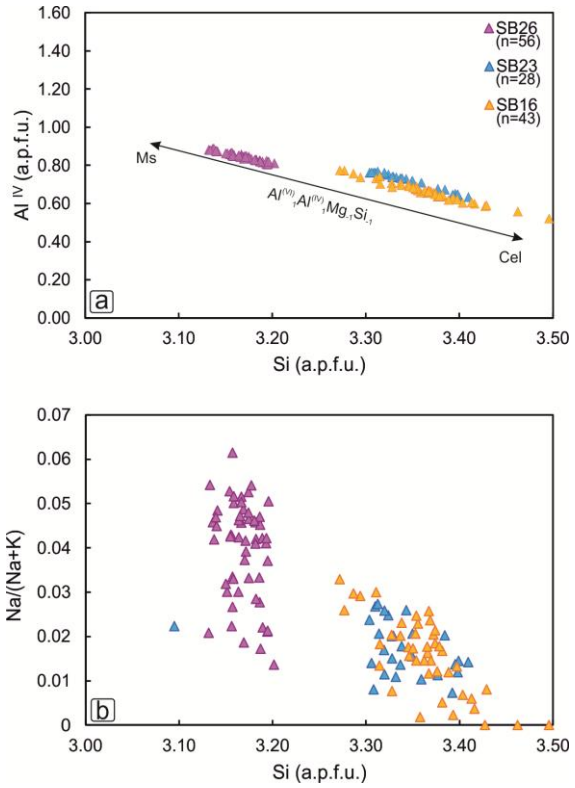

Figure 5. EPMA (Electron Probe Micro Analysis) results showing compositional variation in white mica from orthogneiss samples.

5.2. P-T estimates

Conventional geothermobarometric calculations have been performed on type 1 eclogite samples. As phengite occurs along in the peak equilibrium phase assemblage, the pressure has been estimated using the geothermobarometer of Krogh Ravna and Terry (2004) developed for garnet + omphacite + phengite + kyanite + quartz in the KCMASH system. The Fe-Mg exchange thermometer of Krogh Ravna (2000) has been also applied based on the coexisting clinopyroxene

and garnet stable in the peak metamorphic assemblage. The complete mineral composition dataset has been reported in Figures 4 and 5 and **Table S6.**

Samples SB-5 and SB-35 of the type 1 eclogites and sample SB-3 of type 2 eclogites were used for calculations. Clinopyroxene (Cpx_1 + phengite (Wm_2) and clinopyroxene-garnet-phengite (Cpx_1 + Grt_2 + Wm_2) triplets were selected for the use of the geothermobarometer. All analyses have been performed on mineral grains in textural equilibrium with the eclogitic mylonitic foliation. The peak P-T equilibrium conditions of the eclogites have been determined to be approximately 2.0-2.1 GPa and 520-645 °C.

The P-T isochemical pseudosection has been obtained with the composition of a carbonate-free eclogite sample SB-35 (See "Methods" for details) using the GeoPs software of Xiang and Connolly (2022), based on an algorithm for the minimization of the Gibbs energy. Isopleths for Si (a.p.f.u.) in phengite, Na (a.p.f.u.) in clinopyroxene and *X*Ca, *X*Mg in garnet have been calculated for the HP field of the pseudosection (Figure 6). The calculated phase diagram predicts that the Cpx-free equilibrium phase assemblage preserved in garnet cores (Grt_1 + Wm_1 + Amp_1 + Rt_1 + Qz) is stable below 1.4-1.5 GPa for temperatures lower than 550 °C. Biotite, except for very restricted P-T fields, is predicted as a stable phase, but was never observed as inclusion in Grt_1.

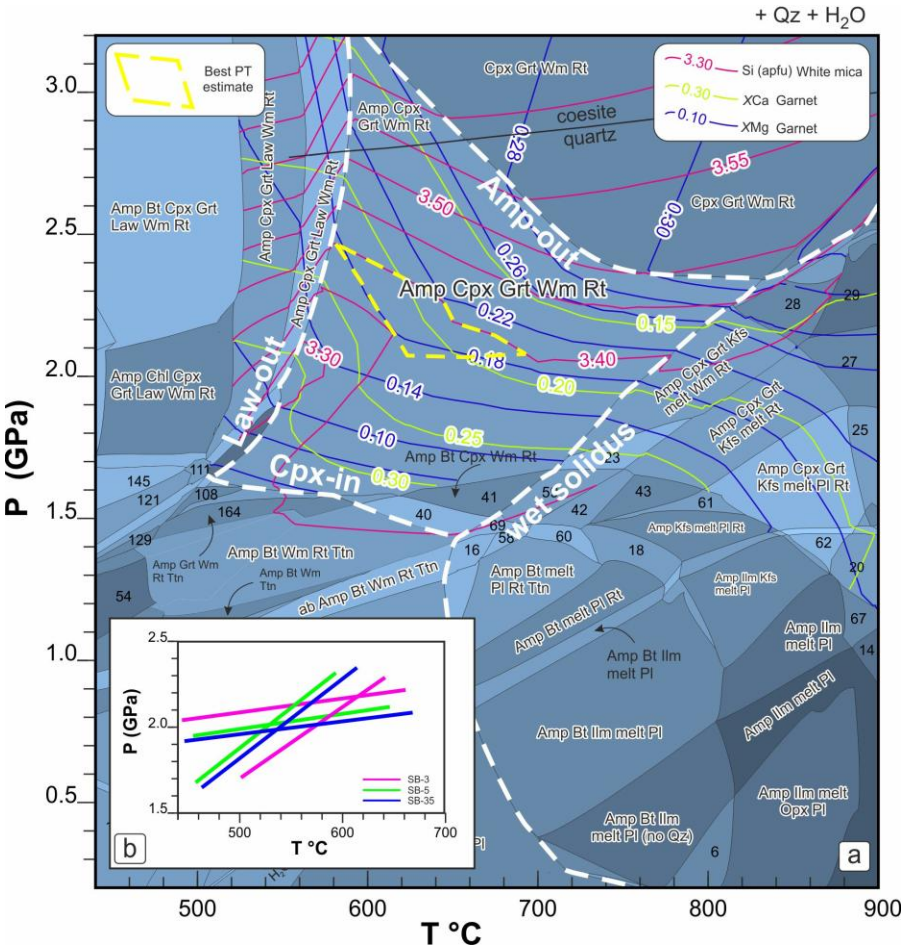

Figure 6. Isochemical phase diagram calculated using the bulk composition of sample SB5. Isopleths for Si in white mica, *X*Ca and *X*Mg in garnet are reported in the stability field of clinpyroxene. Phase assemblages not reported in full are as follows: (6) Pl, Amp, Bt, Chl, Ilm, Ttn; (14) Amp, Cpx, melt Ilm, Pl; (20) Amp, Cpx, Grt, Im, melt, Pl; (25) Amp,

Cpx, Grt, melt, Pl Rt; (27) Amp, Cpx, Grt, Kfs, melt, Rt; (28) Amp, Cpx, Grt, melt, Wm, Rt; (29) Amp, Cpx, Grt, melt, Rt; (40) Amp, Bt, Cpx, Wm, Rt, Ttn; (42) Amp, Bt, Cpx, Kfs, melt, Rt; (43) Amp, Cpx, Kfs, melt, Rt; (54) Amp, Bt, Wm, Ttn; (60) Amp, Bt, Kfs, melt, Rt, Ttn; (61) Amp, Cpx, Kfs, melt, Pl, Rt; (62) Amp, CpxGrt, Ilm, Kfs, melt, Pl; (67) Amp, Cpx, Ilm, melt, Pl; (108) Amp, Grt, Wm, Ttn; (111) Amp, Amp, Grt, Wm, Ttn; (121) Amp, Chl, Grt, Wm, Ttn; (129) Amp, Chl, Grt, Wm, Ttn; (145) Amp, Amp, Chl, Grt, Wm, Ttn; (164) Amp, Chl, Grt, Wm, Rt, Ttn. (b) PT estimates calculated with the Krogh-Ravna and Terry (2004) geothermobarometer for the equilibrium phase assemblage Wm_2 + Cpx_1 + Grt_2.

The syn-mylonitic equilibrium phase assemblage (Grt_2 + Cpx_1 + Wm_2 + Rt_2) is stable at P higher than 2.4 GPa for T > 700 °C, whereas, due to the negative slope of the Amp-out reaction, shift to increasing P as T decreases (Figure 6). Microstructure analysis had shown that blue Na-Ca amphibole (Amp_2), grows subparallel to mylonitic lineation, with a weaker, but still evident SPO, similar in orientation to that of Cpx_1. Amp_2 can thus be considered to have grown during or just after the pressure peak, but still in the P-T field of stability of Na-Clinopyroxene. Considering the Si-content of Wm_2 (Figure 4a-b) and the Grt_2 composition (Figure 4e-f), the isopleths related to these minerals define a P-T range of 580-655 °C and 2.1-2.4 GPa. P-T estimates obtained by conventional geothermobarometry are placed close to the lower P limit defined by the calculated isochemical section, with P of 2.0-2.2 GPa and T of 525-615 °C.

5.3. $^{40}Ar/^{39}Ar$ geochronology

The Ar release pattern of phengitic white mica in all orthogneiss samples is quite identical. Three samples collected from the bottom to the top of E shear zone (Figure 2a) have been dated. The Ar spectrum of the structurally lowest sample, SB-16 (Figure 7), consists of steps 4-8 which comprise 81.7 % of the total ^{39}Ar and show the lowest Ca/K and Cl/K ratios, resulting in an isochemical age of 36.62 ± 0.08 Ma (see **Table S6** for analytical results). SB-23 yields an isochemical age of 33.53 ± 0.10 Ma (steps 4-8 release the 77.9 % of total ^{39}Ar). The isochemical age of SB-26, the closest to the top of the shear zone, is 29.65 ± 0.06 Ma and it is characterized by a flat portion of the spectrum (steps 5-10) with a 85.9 % of ^{39}Ar released and the lowest and homogeneous Ca/K and Cl/K ratios.

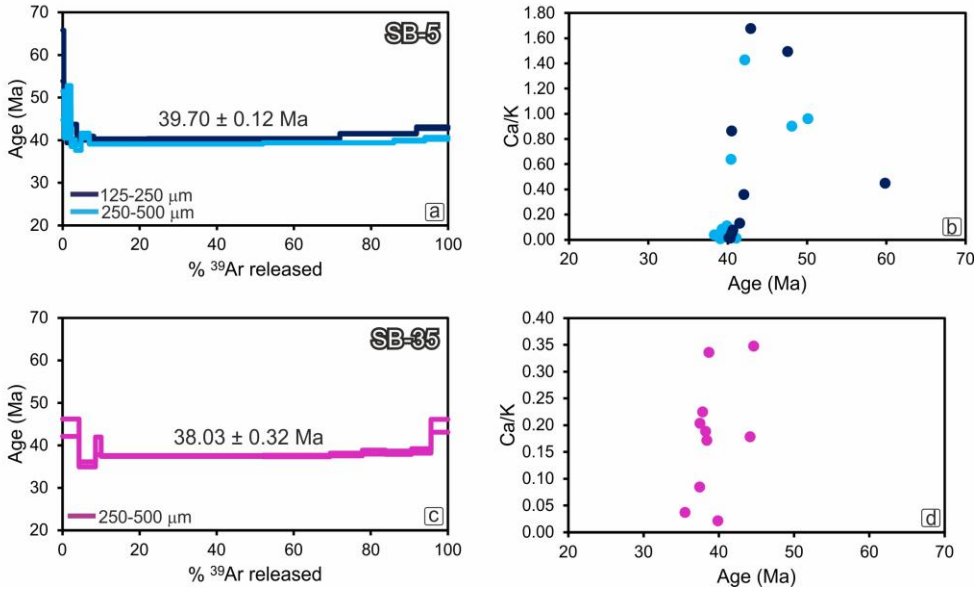

Figure 7. $^{40}Ar/^{39}Ar$ age spectra (mean weighted) and Ca/K vs. age diagrams for eclogite SB-5 (a, b) and SB-35 (c, d). The mean weighted age and dated fraction size have been reported for each sample.

In two eclogite samples the phengitic white mica (Wm_2) along the mylonitic foliation have been dated. For sample SB5 two distinct mica fractions have been dated (125-250 µm and 250-500 µm) to check the possible effect of diffusion during retrogression (e.g. Montemagni and Villa, 2021). The two fractions display similar release patterns, with more than 90 % ^{39}Ar released in the last four steps (7-10). The obtained ages are 39.70 ± 0.12 Ma for both the 250-500 µm and the 125-250 µm fractions. For sample SB-35 a single fraction has been separated and measured, providing an age of 38.03 ± 0.32 Ma (85.5 % of total ^{39}Ar, step 4-9, Figure 8).

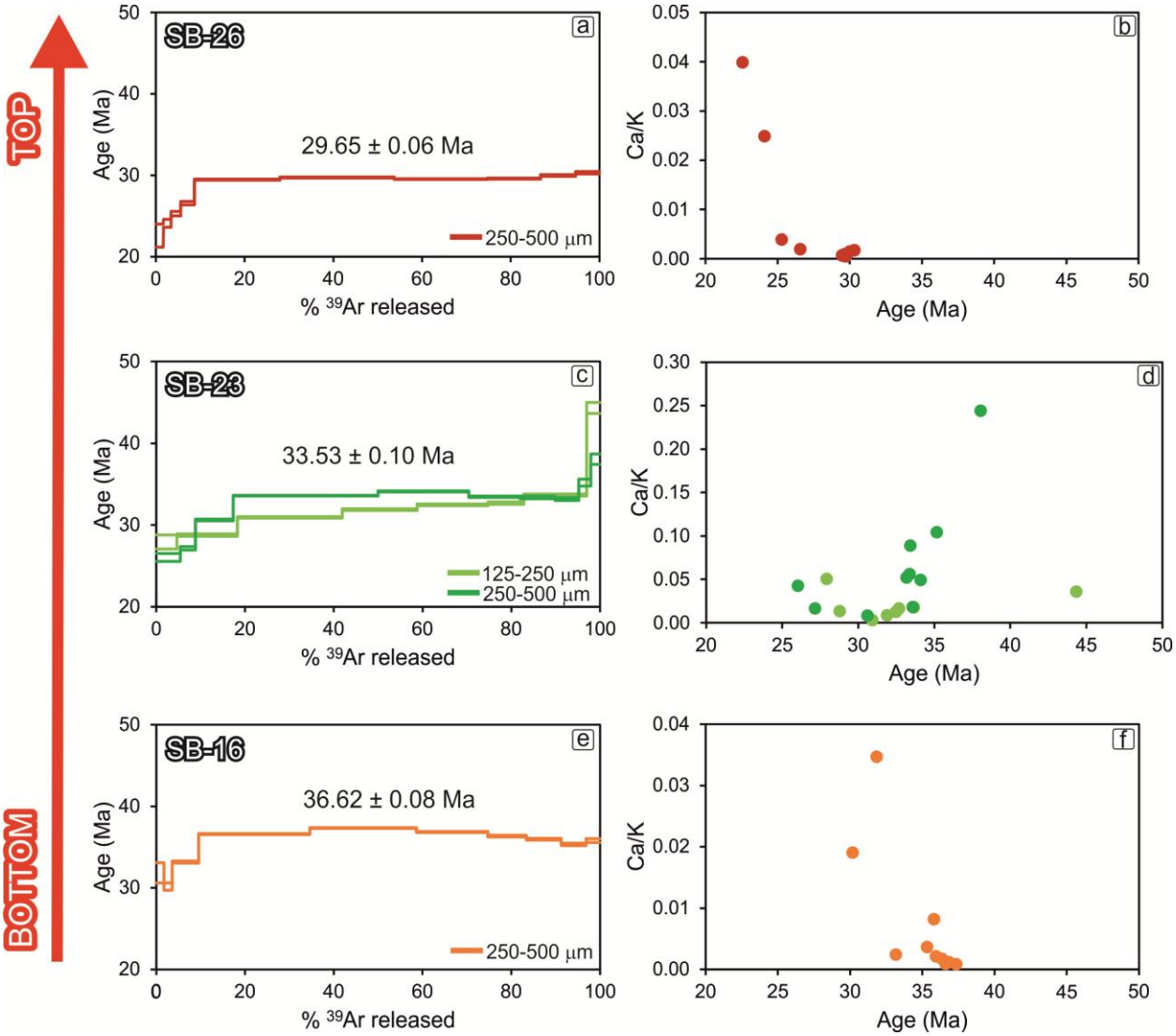

Figure 8. $^{40}Ar/^{39}Ar$ age spectra with obtained mean weighted age and Ca/K vs. age diagrams for orthogneiss SB-26 (a, b), SB-23 (c, d) and SB-16 (e, f). The dated fraction size has been reported for each sample.

6 Discussion

The eclogite bodies of the Adula unit have been studied for a long time since they represent key rocks to understand the pre-Alpine and Alpine subduction-related processes (Figure 9, Liati et al., 2009; Herwartz et al., 2011).

The eclogite bodies of southern Adula have Alpine ages while in northern Adula they carry pre-Alpine ages (Figure 9b, Liati et al., 2009). Until now, Alpine HP metamorphism had been traced as far north as the Trescolmen locality (Tr in Figure 1b), where Alpine eclogites also preserve HP Variscan relicts (Herwartz et al., 2011). This study provides the first dating of the San Bernardino eclogites, yielding an age of 38-39 Ma. These results extend the documented northern limit of Alpine HP metamorphism within the Adula nappe. The consistent peak pressure ages (38-43 Ma) and metamorphic conditions (600-650 °C and 2.0-2.5 GPa; Brouwer et al., 2005) suggest that at least the southern half of the Adula unit behave as a coherent crustal block during the Alpine subduction and exhumation.

Atop the Adula unit, in the San Bernardino Pass area, the SBSZ is a c. 500 m thick extensional top-to-the-NE shear zone showing an increasing strain gradient toward the east, namely from the bottom to the top of the SBSZ. Only a faint NE to E-trending lineation is observable in the lower portion of the shear zone, where the dominant top-to-the-NW shear fabric prevails. This top-to-the-NW shear fabric is also pervasive in the entire Adula nappe (Nagel, 2008) and related to the nappe stacking event during the Zapport phase (36-33 Ma, Pleuger et al., 2003). Only a partial overprint of the top-to-the-NE shearing is visible both at the meso- and microscale, resulting in the growth of a second mica generation (Wm_2), that in turn led to mixed deformation ages, which indicates the maximum age (36 Ma) for the onset of shearing. Approaching the top of the shear zone, the top-to-the-NE related fabric of the SBSZ becomes more pronounced, with Wm_2 that recrystallized along L_3 NE-trending lineation, substituting Wm_1 in orthogneisses (Figure 3). The eastward progressive overprinting of L_3 on L_2 coincides with the younging trend of mica ages: the youngest age (29 Ma, Figure 7) can be considered the maximum age for the onset of top-to-the-E extensional shearing along the SBSZ.

We argue that the crustal extension accommodated by the SBSZ is responsible for part of the exhumation of the eastern flank of the Lepontine Dome, the Ticino culmination (Figures 1a and 9a). Top-to-the-E shearing was not confined to the Middle Penninic nappes or the contact between the Upper Penninic and Austroalpine units (e.g. Avers-Turba Mylonite Zone and Martegnas Shear Zone reported in Ring & Glodny, 2021; Berger et al., 2005; Frey & Ferreiro Mählmann, 1999; Nagel, 2008; Rosenberg et al., 2021; Todd & Engi, 1997), but also affected the Adula unit. Our results support the hypothesis proposed by Ring and Glodny (2021), which suggests that the top-to-the-SE ductile extensional shearing was progressively activated from east to west and from top to bottom in the nappe pile. This shearing initially occurred in the Upper Penninic mylonite zones (the Avers-Turba and Martegnas mylonite zones, Ring & Glodny, 2021), before migrating to the Middle Penninic Splügen and Misox zones (Figure 1b), where it reached the top of the Adula nappe.

Top-to-the-SE ductile shearing began around 45 Ma, while the Lower Penninic units had yet to reach peak-pressure conditions. The waning stage of this shearing in the Upper and Middle Penninic units persisted until 34 Ma (Price et al., 2018; Ring & Glodny, 2021), just before the peak

467 temperature of the amphibolite facies metamorphism in the Lepontine Dome at 33-31 Ma (e.g.
468 Tagliaferri et al., 2023). Younger ages associated with top-to-the-E extensional shearing (35-31
469 Ma, Ring & Glodny, 2021) occur in the Splügen and Misox Zone, corresponding to an intra-Middle
470 Penninic shear zone and to the contact between the Middle and the Lower Penninic nappe stack,
471 respectively.

472 The 39-38 Ma age of the San Bernardino eclogites confirms that the Adula nappe reached HP
473 conditions while top-to-the-SE ductile shearing was active in the upper levels of the growing
474 orogenic wedge. The onset of top-to-the-NW nappe stacking is broadly coeval with the
475 deactivation of the top-to-the-SE extensional shearing in the Upper Penninic structures and its
476 westward migration, slightly rotating to a top-to-the-E direction (Ring & Glodny, 2021).

477 The top-to-the-NW nappe-stacking of the Lower Penninic units in the Lepontine Dome occurred
478 in the 36-34 Ma time interval (e.g. Nagel, 2008; Steck et al., 2019), and it was largely coeval with
479 amphibolite facies regional metamorphism, leading to widespread crustal anatexis in the
480 Southern Steep Belt (Figure 1a-b) and local migmatization along the main tectonic contacts in the
481 southern and central part of the dome (Tagliaferri et al., 2023). Crustal shortening and thrusting
482 of the Lower Penninic HP units above the non-HP units occurred at the same time with orogen-
483 parallel extension, which reduced overburden in the growing Lepontine nappe-stack. As the HP
484 units were exhumed, top-to-the-E shearing progressively migrated downward, affecting the
485 Splügen Zone, the base of the Suretta nappe and the Misox Zone before finally activating the
486 SBSZ at ca. 29 Ma, based on our data. The new age of the top-to-the-E mylonites at the top of
487 the Adula nappe point to a distributed top-to-the-E shearing reaching the exhuming HP units of
488 the Lepontine Dome by the middle to late Oligocene.

489 However, the role of orogen-parallel extension during Adula nappe exhumation remains
490 debated. Classical models (e.g., Schmid et al. 1996; Rosenberg et al. 2021) suggest minor or
491 negligible extension, whereas others (Marquer et al., 1996; Pleuger et al., 2003; Ring & Glodny,
492 2021) argue for a penetrative, long-lasting orogen-parallel extension.

493 Contrary, in the western flank of the Lepontine Dome, the exhumation of the Toce culmination
494 was fostered by the younger Simplon Fault (Figures 1a and 9a) in the 20-8 Ma time span
495 (Montemagni & Zanchetta, 2022, with references). Some Authors (Meyre et al., 1998;
496 Schlunegger & Willett, 1999), based on similar amount of syn-orogenic extension and age of
497 shearing, proposed that the Forcola Fault (21-18 Ma), the southeastward continuation of the
498 Misox Zone (Figure 1), represents the eastern equivalent of the Simplon Fault. However, the
499 offset of the metamorphic isograds across the Simplon Fault point to a vertical displacement of
500 about 15 km (Grasemann & Mancktelow, 1993), whereas no comparable offset is observed
501 across the Forcola Fault (Frey & Ferreiro-Mählmann, 1999; Ciancaleoni & Marquer, 2008)
502 suggesting that the exhumation of the Lepontine Dome is mainly accommodated by localized
503 normal shearing in the west, and by more local tilting, doming and normal shearing and faulting
504 along several structures and nappe-separating metasediments zones (i.e. Misox Zone and
505 Splügen Zone) within Penninic and Austroalpine nappe stack in the east (Rahn, 2005).

506 Over a short time span (< 5 Myrs), the Adula unit experienced HP metamorphism during south
507 dipping continental subduction, developing eclogites at 2-2.5 GPa around 40 Ma in the central-
508 northern portion of the slab (Figure 9b, e), followed by a rapid top-to-the-NW directed

exhumation (Figure 9c) during the nappe-stacking phase (33-36 Ma, Wiederkher et al., 2008, 2009). Top-to-the-E ductile shearing occurred in the hanging wall of the Misox Zone since at least 45 Ma, testifying for the contemporaneity of orogen-perpendicular shortening and orogen-parallel extension., the last promoting the exhumation of the Adula itself in the 36-29 Ma time span (Figure 9d).

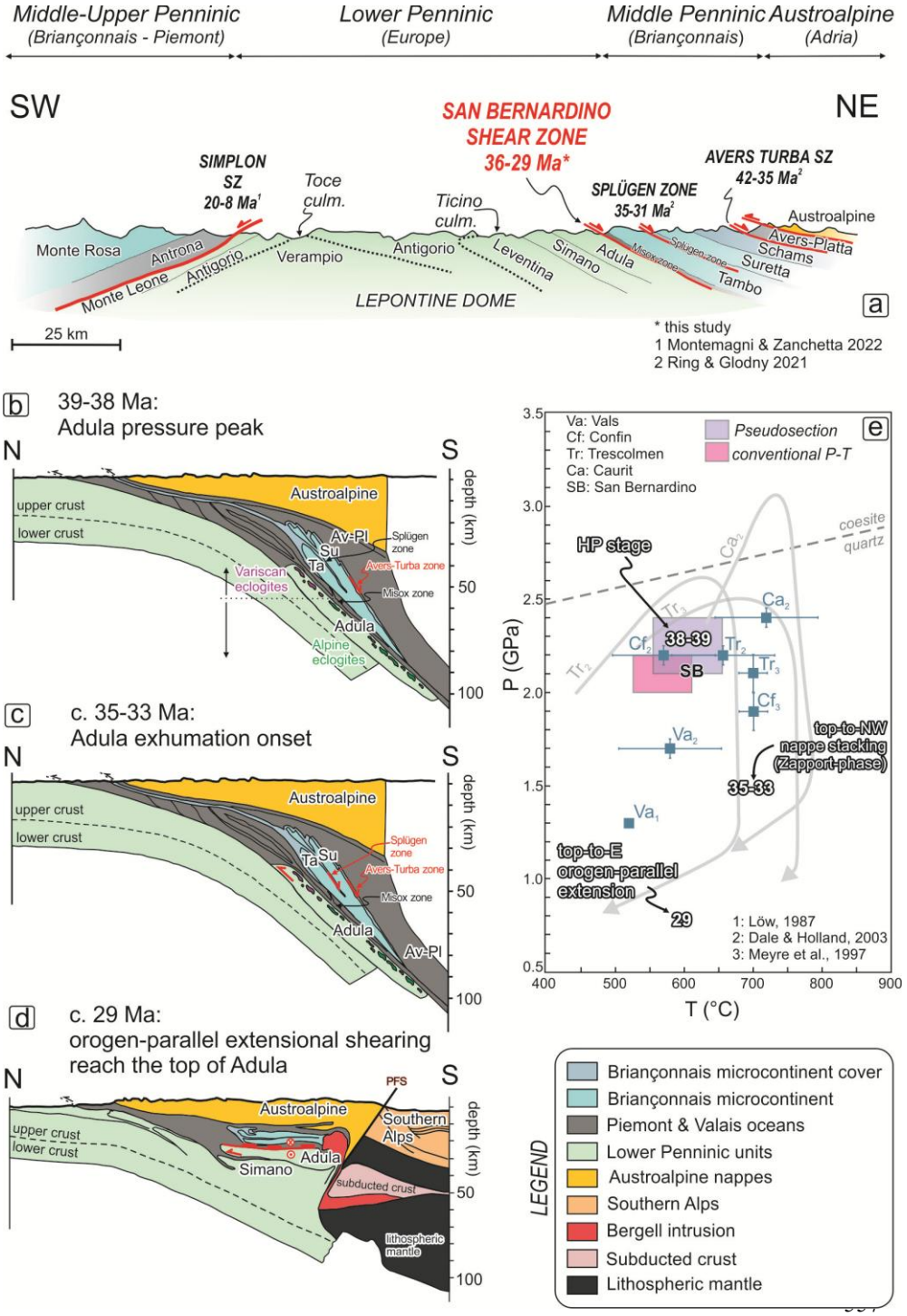

Figure 9. (a) Structural cross-section through the Lepontine dome (modified from Steck et al., 2013) with shear zones at the western and eastern flank of the dome highlighted. (b-d) Tectonic interpretation (after Ring & Glodny, 2021).

(b) At 39-38 Ma the Adula reached the pressure peak conditions. The Avers-Turba mylonite zone was active. Eclogites are indicated: violet for Variscan eclogites and green for Alpine eclogites. (c) Beginning of overthrusting during the coherent exhumation of the Adula unit onto the underlying nappes. In this stage the Splügen zone is also active. (d) At c. 29 Ma the orogen-parallel extensional shearing reached the top of the Adula unit, partially coeval with thrusting at the bottom of the unit itself. (e) P-T estimates and P-T paths for various localities in the Adula unit. Violet and pink squares indicates the P-T estimates obtained in this study, *via* pseudosection and conventional P-T respectively. The ages for HP metamorphism, exhumation and orogen-parallel extension have been reported.

A similar tectonic framework is observed in the Eastern Alps, where the exhumation of the Tauern Window was accommodated by the Brenner Shear Zone in the west and the Katschberg Shear Zone in the east, which exhibited top-to-the-W and top-to-the-E extensional ductile shearing, respectively, since about 25 Ma (e.g. Steck, 1984; Ratschbacher et al., 1991). Hence, as the Tauern Window in the Eastern Alps, the Lepontine Dome in the Central Alps, experienced syn to post-collisional orogen-parallel extensional shearing, facilitating the exhumation of the (U)HP units currently exposed in the Penninic nappe-stack of the Central Alps.

Nevertheless, the extent, duration, and role of orogen-parallel extension in the evolution of convergent plate margins remain debated (Beltrando et al., 2010; Rosenberg & Garcia, 2011). Tectonic switching between orogen-perpendicular lithospheric thickening and orogen-parallel lithospheric thinning has been invoked to explain the evolution of the Oligocene Central Alps (Beltrando et al., 2010). Crustal scale extension within a developing orogenic wedge may emerge as a transient yet dominant deformation style across the entire orogen, driven by episodic lithospheric thinning due to geodynamic changes such as slab rollback, change in convergence velocity and relative motion between the hinge of the subducting slab and the leading edge of the upper plate.

Traditionally, the structural evolution of the Alps has been interpreted through orogenic wedge models, where nappes formed at crustal depths *via* ductile underthrusting at the base of the wedge (e.g. Platt 1986). However, the discovery of (U)HP rocks recording pressures far exceeding the pressures predicted by orogenic wedge models (see Jolivet et al., 2003), has led to alternative hypotheses to explain the structural evolution of Central Alps. These hypotheses include buoyancy-driven exhumation, which can occur through three main mechanisms: (i) continuous return flow of rocks within a subduction channel, (ii) upward flow of individual buoyant rock units through denser material, and (iii) lithospheric extension and associated upward flow due to slab rollback (Schenker et al., 2015 with references). Our data support the hypothesis that the final exhumation of the Adula unit was driven by top-to-the-E extensional shearing, which distinctly began before 30 Ma, broadly coeval with the emplacement of the Bergell pluton at ca. 20 km depth between 32 and 28 Ma (e.g. von Blanckenburg, 1992). As the Lepontine Dome was tectonically exhumed, top-to-the-E shearing progressively migrated to deeper structural levels, reaching the top of the Adula nappe at ca. 30 Ma.

The evolution of the SBSZ must be considered within the broader dynamics of the Alpine orogenic wedge. During convergence the HP peak (~2.0-2.4 GPa, 580-655 °C at 38-39 Ma) was rapidly followed by top-to-the-NW nappe stacking, reflecting critical taper conditions in a compressive wedge. However, as burial peaked and crustal thickening progressed, the system transitioned into a gravitationally unstable configuration, prompting a switch to orogen-parallel extension.

The activation of top-to-the-E extensional shear zones such as the SBSZ illustrates this shift in kinematics captured in the progressive overprinting of early fabrics and the partial to complete resetting of $^{40}Ar/^{39}Ar$ mica ages to 29 Ma. This transition was likely driven by a combination of slab rollback, lower crustal flow, and thermally induced weakening from crustal melting. Such dynamic orogenic feedbacks promoted a rapid switch from crustal accretion to ductile thinning and exhumation. The contemporaneity of amphibolite-facies metamorphism and extensional fabrics supports a model in which, intrusion of Bergell pluton (32-28 Ma) and extension were coeval yet partitioned, reflecting a complex interplay between deep burial, magma emplacement, lateral extrusion, and surface uplift in an evolving orogenic wedge.

7 Conclusions

This study presents new constraints on the tectonometamorphic evolution of the Adula unit in the eastern Central Alps, focusing on the San Bernardino Pass area. Through integrated structural, petrological, thermodynamic modelling, and $^{40}Ar/^{39}Ar$ geochronological analyses, we document the first occurrence of Alpine high-pressure metamorphism in the northern sector of the Adula nappe. $^{40}Ar/^{39}Ar$ dating of synkinematic phengitic white mica yields consistent ages of 38-39 Ma, coinciding with peak metamorphic conditions of 2.0-2.4 GPa and 580-655 °C.

The extensional San Bernardino Shear Zone (SBSZ), a top-to-the-E ductile shear zone, is developed within the upper Adula unit and accommodated part of the unit exhumation. Progressive textural overprinting of top-to-the-NW nappe-stacking fabrics (Zapport phase) by top-to-the-E mylonitic fabrics related to the SBSZ, is matched by a progressive $^{40}Ar/^{39}Ar$ age resetting with L_3 lineation associated to the synkinematic growth of a second white mica generation in orthogneisses, marking the transition from crustal shortening to extensional shearing.

The combination of petrochronological and structural data highlights a rapid tectonic evolution from subduction (~39 Ma), through nappe stacking (36–34 Ma), to final exhumation along extensional shear zone (~30 Ma), within a timeframe of less than 10 Myrs.

This transition reflects a major shift in orogenic dynamics—from compressive crustal thickening under critical taper conditions to gravitational collapse and orogen-parallel extension. The onset of extensional shearing in the SBSZ was likely triggered by slab rollback and lower crustal flow, that, together with thermal weakening from partial melting, created a dynamically unstable orogenic wedge. Notably, the contemporaneity of amphibolite-facies metamorphism and the emplacement of the Bergell pluton (~32–28 Ma) with top-to-the-E shearing suggests partitioned yet genetically linked processes of exhumation and magmatism.

These results support a model in which the eastern Lepontine Dome was exhumed via distributed orogen-parallel extension along several shear zones activating from upper structural levels downwards, reaching the top of the Adula unit at ~30 Ma.

The consistent metamorphic conditions and timing across the unit suggest that the Adula unit behaved as a coherent crustal block during Alpine subduction and exhumation.

Acknowledgments

C. Montemagni, N. Malaspina and S. Zanchetta acknowledge the support of Project MUR – Dipartimento di Eccellenza 2023-2027 "TECLA" (Grant n. 2023-NAZ-0212). We thank A. Risplendente (University of Milano) for the EMPA sessions.
The contact author declares that none of the authors has any competing interests.

Data Availability Statement

EMPA and $^{40}Ar/^{39}Ar$ data are available in a free-access repository (doi: 10.17632/hctf2rgcnk.1).

References

Becker, H. (1993). Garnet peridotite and eclogite Sm-Nd mineral ages from the Lepontine dome (Swiss Alps): New evidence for Eocene high-pressure metamorphism in the central Alps. *Geology*, *21*(7), 599–602. https://doi.org/10.1130/0091-7613(1993)021<0599:GPAESN>2.3.CO;2.

Beltrando, M., Lister, G. S., Rosenbaum, G., Richards, S., & Forster, M. A. (2010). Recognizing episodic lithospheric thinning along a convergent plate margin: The example of the Early Oligocene Alps. *Earth Science Review, 103*, 81-98.

Berger, A., Mercolli, I., & Engi, M. (2005). The central Lepontine Alps: notes accompanying the tectonic and petrographic map sheet Sopra Ceneri (1:100,000). *Schweizerische Mineralogische und Petrographische Mitteilungen, 85*, 109–146.

Brouwer, F. M., Burri, T., Engi, M., & Berger, A. (2005). Eclogite relics in the Central Alps: PT-evolution, Lu-Hf ages and implications for formation of tectonic mélange zones. *Schweizerische Mineralogische und Petrographische Mitteilungen, 85*, 147–174.

Burri, T., Berger, A., & Engi, M. (2005). Tertiary migmatites in the Central Alps: regional distribution, field relations, conditions of formation, and tectonic implications. *Schweizerische Mineralogische und Petrographische Mitteilungen*, *85*, 215-232.

Cavargna-Sani, M., Epard, J. L., & Steck, A. (2014). Structure, geometry and kinematics of the northern Adula nappe (Central Alps). *Swiss Journal of Geosciences, 107*, 135–156. https://doi.org/10.1007/s00015-014-0175-7.

Cawthorn, R. G., & Collerson, K. D. (1974). The recalculation of pyroxene endmember parameters and the estimation of ferrous and ferric iron content from electron microprobe analyses. *American Mineralogist, 59*(11-12), 1203–1208.

Chemenda, A. I., Mattauer, M., Malavieille, J., & Bokun, A. N. (1995). A mechanism for syn-collisional rock exhumation and associated normal faulting: results from physical modelling. *Earth and Planetary Science Letters, 132*, 225–232.

Ciancaleoni, L., & Marquer, D. (2008). Late Oligocene to early Miocene lateral extrusion at the eastern border of the Lepontine Dome of the Central Alps (Bergell and Insubric areas, eastern Central Alps). *Tectonics, 27*, TC4008. https://doi.org/10.1029/2007TC002196.

Dale, J., & Holland, T. J. B. (2003). Geothermobarometry, P–T paths and metamorphic field gradients of high-pressure rocks from the Adula Nappe, Central Alps. *Journal of Metamorphic Geology, 21,* 813–829. https://doi.org/10.1046/j.1525-1314.2003.00483.x.

Dewey, J. F., Helman, M. L., Knott, S. D., Turco, E., & Hutton, D. H. W. (1989). Kinematics of the western Mediterranean. *Geological Society of London Special Publications, 45*(45), 265–283. https://doi.org/10.1144/GSL.SP.1989.045.01.15.

Engi, M., Berger, A., & Roselle, G. T. (2001). Role of the tectonic accretion channel in collisional orogeny. *Geology, 29*, 1143–1146.

Evans, B. W., & Trommsdorff, V. (1978). Petrogenesis of garnet lherzolite, Cima di Gagnone, Lepontine Alps. *Earth and Planetary Science Letters*, *40*(3), 333–348. https://doi.org/10.1016/0012-821x(78)90158-9.

Faryad, S., Klápová, H., & Nosál, L. (2010). Mechanism of formation of atoll garnet during high-pressure metamorphism. *Mineralogical Magazine, 74*, 111-126.

Federico, L., Crispini, L., Scambelluri, M., & Capponi, G. (2007). Ophiolite mélange zone records exhumation in a fossil subduction channel. *Geology, 35*, 499–502.

Frey, M., & Ferreiro Mählmann, R. (1999). Alpine metamorphism of the Central Alps. *Schweizerische Mineralogische und Petrographische Mitteilungen, 79*(1), 135–154.

Galster, F., Cavargna-Sani, M., Epard, J. L., & Masson, H. (2012). New stratigraphic data from the Lower Penninic between the Adula nappe and the Gotthard massif and consequences for the tectonics and the paleogeography of the central Alps, *Tectonophysics*, *579*, 37–55.

Gebauer, D. (1996). A P-T-t path for an (ultra?-) high-pressure ulramafic/mafic rock-association and its felsic country-rocks based on SHRIMP-dating of magmatic and metamorphic zircon domains. Example: Alpe Arami (Central Swiss Alps). In Earth Processes Reading the Isotopic Code, Geophysical Monograph (Vol. 95, pp. 307–329). American Geophysical Union.

Gerya, T. V., Stöckhert, B., & Perchuk, A. L. (2002). Exhumation of high-pressure metamorphic rocks in a subduction channel: a numerical simulation. *Tectonics, 21*, TC1056.

Grasemann, B., & Mancktelow, N. S. (1993). Two-dimensional thermal modelling of normal faulting: the Simplon Fault zone, central alps, Switzerland. *Tectonophysics, 225*, 155–165. https://doi.org/10.1016/0040-1951(93)90277-Q.

Green, E. C. R., White, R. W., Diener, J. F. A., Powell, R., Holland, T. J. B., & Palin, R. M. (2016). Activity–composition relations for the calculation of partial melting equilibria in metabasic rocks. *Journal of Metamorphic Geology, 34*(9), 845-869.

Hacker, B. R., & Gerya, T. V. (2013). Paradigms, new and old, for ultrahigh-pressure tectonism. *Tectonophysics,* 603, 79–88.

714 Handy, M. R., Schmid, S. M., Bousquet, R., Kissling, E., & Bernoulli, D. (2010). Reconciling
715 plate-tectonic reconstructions of Alpine Tethys with the geological–geophysical record of
716 spreading and subduction in the Alps. *Earth Science Reviews, 102*(3-4), 121-158.

717 Hawthorne, F. C., & Oberti, R. (2007). Classification of the amphiboles. *Reviews in*
718 *Mineralogy and Geochemistry*, *67*(1), 55–88.

719 Heinrich, C. A. (1986). Eclogite facies regional metamorphism of hydrous mafic rocks in the
720 Central Alpine Adula Nappe. *Journal of Petrology, 27*(1), 123–154.
721 https://doi.org/10.1093/petrology/27.1.123.

722 Hermann, J., Rubatto, D., & Trommsdorff, V. (2006). Sub-solidus Oligocene zircon formation
723 in garnet peridotite during fast decompression and fluid infiltration (Duria, Central Alps).
724 *Contributions to Mineralogy and Petrology, 88*, 181-206.

725 Herwartz, D., Nagel, T. J., Münker, C., Scherer, E. E., & Froitzheim, N. (2011). Tracing two
726 orogenic cycles in one eclogite sample by Lu-Hf garnet chronometry. *Nature Geoscience,*
727 *4*(3), 178–183. https://doi.org/10.1038/ngeo1060.

728 Holland, T. J. B., & Powell, R. (1998). An internally consistent thermodynamic data set for
729 phases of petrological interest. *Journal of Metamorphic Geology,* 16, 309–343.

730 Holland, T. J. B., & Powell, R. (2011). An improved and extended internally consistent
731 thermodynamic dataset for phases of petrological interest, involving a new equation of
732 state for solids. *Journal of Metamorphic Geology,* 29, 333–383.

733 Jolivet, L., Faccenna, C., Goffe, B., Burov, E., & Agard, P. (2003). Subduction tectonics and
734 exhumation of high-pressure metamorphic rocks in the Mediterranean orogens. *American*
735 *Journal of Science, 303*(5), 353-409.

736 Kossak-Glowczewski, J., Froitzheim, N., Nagel, T. J., Pleuger, J., Keppler, R., Leiss, B., &
737 Régent, V. (2017). Along-strike shear-sense reversal in the Vals-Scaradra Shear Zone at the
738 front of the Adula Nappe (Central Alps, Switzerland). *Swiss Journal of Geosciences*, *110*,
739 677-697.

740 Krogh Ravna, E. J. (2000). The garnet–clinopyroxene Fe2þ–Mg geothermometer: an
741 updated calibration. *Journal of Metamorphic Geology, 18*(2), 211–219.

742 Krogh Ravna, E. J., & Terry, M. P. (2004). Geothermobarometry of UHP and HP eclogites
743 and schists - an evaluation of equilibria among garnetclinopyroxene- kyanite-phengite-
744 coesite/quartz. *Journal of Metamorphic Geology,* 22(6), 579–592.

745 Liati, A., Gebauer, D., & Fanning, C. M. (2009). Geochronological evolution of HP
746 metamorphic rocks of the Adula nappe, Central Alps, in pre-Alpine and Alpine subduction
747 cycles. *Journal of the Geological Society, 166*(4), 797–810. https://doi.org/10.1144/0016-
748 76492008-033.

749 Malusà, M. G., Faccenna, C., Baldwin, S. L., Fitzgerald, P. G., Rossetti, F., Balestrieri, M. L.,
750 Danišík, M., Ellero, A., Ottria, G., & Piromallo, C. (2015). Contrasting styles of (U) HP rock
751 exhumation along the Cenozoic Adria-Europe plate boundary (Western Alps, Calabria,
752 Corsica). *Geochemistry, Geophysics, Geosystems,* 16(6), 1786-1824.

753 Mancktelow, N. S. (1985). The Simplon Line: a major displacement zone in the western
754 Lepontine Alps. *Eclogae Geologicae Helvetiae, 78*, 73–96.

755 Marquer, D., Challandes, N., & Baudin, T. (1996). Shear zone patterns and strain distribution
756 at the scale of a Penninic nappe: the Suretta nappe (Eastern Swiss Alps). *Journal of*
757 *Structural Geology*, *18*, 753–764.

758 Merle, O, & Guillier, B. (1989). The building of the Swiss Central Alps: an experimental
759 approach. *Tectonophysics*, *165*, 41–56.

760 Meyre, C., Marquer, D., Schmid, S. M., & Ciancaleoni, L. (1998). Syn-orogenic extension
761 along the Forcola fault: Correlation of alpine deformations in the Tambo and Adula nappes
762 (eastern Penninic Alps). *Eclogae Geologicae Helvetiae*, *91*(3), 409–420.

763 Montemagni, C., & Villa, I.M. (2021). Geochronology of Himalayan shear zones: unravelling
764 the timing of thrusting from structurally complex fault rocks. *Journal of the Geological*
765 *Society*, *178*, 1–13. https://doi.org/10.1144/jgs2020-235.

766 Montemagni, C., & Zanchetta, S. (2022). Constraining kinematic and temporal evolution of
767 a normal-sense shear zone: insights into the Simplon Shear Zone (Western Alps). *Journal of*
768 *Structural Geology*, *156*, 104557. https://doi.org/10.1016/j.jsg.2022.104557

769 Nagel, T. J. (2008). Tertiary subduction, collision and exhumation recorded in the Adula
770 nappe, central Alps. *Geological Society of London Special Publications, 298*(1), 365–392.
771 https://doi.org/10.1144/sp298.17.

772 Nagel, T. J., De Capitani, C., & Frey, M. (2002). Isograds and P-T evolution in the eastern
773 Lepontine Alps (Graubünden, Switzerland). *Journal of Metamorphic Geology,* 20(3), 309–
774 324. https://doi.org/10.1046/j.1525-1314.2002.00368.x.

775 Passchier, C. W., & Trouw, R. A. J. (2005). Microtectonics. Springer Verlag, Berlin.

776 Piccoli, F., Lanari, P., Hermann, J., & Pettke, T. (2022). Deep subduction, melting, and fast
777 cooling of metapelites from the Cima Lunga Unit, Central Alps. *Journal of Metamorphic*
778 *Geology,* 40(1), 121-143.

779 Platt, J. P. (1986). Dynamics of orogenic wedges and the uplift of high-pressure
780 metamorphic rocks. *Geological Society of America Bulletin, 97*, 1037–1053.

781 Pleuger, J., Hundenborn, R., Kremer, K., Babinka, S., Kurz, W., Jansen, E., & Froitzheim, N.
782 (2003). Structural evolution of Adula nappe, Misox zone, and Tambo nappe in the San
783 Bernardino area: Constraints for the exhumation of the Adula eclogites. *Österreichischen*
784 *Geologischen Gesellschaft, 94*, 99–122.

785 Pleuger, J., Nagel, T. J., Walter J. M., Jansen, E., & Froitzheim, N. (2008). On the role and
786 importance of orogen-parallel and -perpendicular extension, transcurrent shearing, and
787 backthrusting in the Monte Rosa nappe and the Southern Steep Belt of the Alps (Penninic
788 zone, Switzerland and Italy). *Geological Society of London Special Publications, 298*, 251-
789 280.

Price, J. B., Wernicke, B. P., Cosca, M. A., & Farley, K. A. (2018). Thermochronometry across the Austroalpine-Pennine boundary, Central Alps, Switzerland: Orogen-Perpendicular Normal Fault Slip on a Major "Overthrust" and its implications for orogenesis. *Tectonics, 37*, 724–757. https://doi.org/10.1002/2017TC004619.

Rahn, M. K. (2005). Apatite fission track ages from the Adula nappe: late-stage exhumation and relief evolution. *Schweizerische Mineralogische und Petrographische Mitteilungen, 85,* 233-245.

Ratschbacher, L., Frisch, W., Linzer, H.-G., & Merle, O. (1991). Lateral extrusion in the Eastern Alps; part 2, Structural analysis. *Tectonics, 10*, 257–271.

Ring, U., & Glodny, J. (2021). The importance of tangential motion in the Central Alps: Kinematic analysis and RbSr dating of mylonitic rocks from the Pennine nappes in the eastern Central Alps. *Earth Science Reviews, 218*, 103644. https://doi.org/10.1016/j.earscirev.2021.103644.

Rosenberg, C. L., Bellahsen, N., Rabaute, A., & Girault, J. B. (2021). Distribution, style, amount of collisional shortening, and their link to Barrovian metamorphism in the European Alps. *Earth Science Reviews, 222*, 103774. https://doi.org/10.1016/j.earscirev.2021.103774.

Rosenberg, C. L., & Garcia, S. (2011). Estimating displacement along the Brenner Fault and orogen-parallel extension in the Eastern Alps. *International Journal of Earth Sciences, 100*, 1129-1145.

Rubatto, D., Regis, D., Hermann, J., Boston, K., Engi, M., Beltrando, M., & McAlpine, S. R. B. (2011). Yo-yo subduction recorded by accessory minerals in the Italian Western Alps. *Nature Geoscience, 4*, 338–342.

Sandmann, S., Nagel, T. J., Herwartz, D., Fonseca, R. O. C., Kurzawski, R. M., Münker, C., & Froitzheim, N. (2014). Lu–Hf garnet systematics of a polymetamorphic basement unit: new evidence for coherent exhumation of the Adula Nappe (Central Alps) from eclogite-facies conditions. *Contributions to Mineralogy and Petrology, 168*, 1075. https://doi.org/10.1007/s00410-014-1075-6

Scambelluri, M., Pettke, T., Rampone, E., Godard, M., & Reusser, E. (2014). Petrology and trace element budgets of high-pressure peridotites indicate subduction dehydration of serpentinized mantle (Cima di Gagnone, Central Alps, Switzerland). *Journal of Petrology,* 55(3), 459-498.

Schenker, F. L., Schmalholz, S. M., Moulas, E., Pleuger, J., Baumgartner, L. P., Podladchikov, Y., Vrijmoed, J., Buchs, N., & Müntener, O. (2015). Current challenges for explaining (ultra) high-pressure tectonism in the Pennine domain of the Central and Western Alps. *Journal of Metamorphic Geology,* 33(8), 869-886.

Schlunegger, F., & Willett, S. (1999). Spatial and temporal variations in exhumation of the central Swiss Alps and implications for exhumation mechanisms. *Geological Society of London Special Publications*, *154*(1), 157-179, https://doi.org/10.1144/GSL.SP.1999.154.01.07

Schmid, S. M., Fügenschuh, B., Kissling, E., & Schuster, R. (2004). Tectonic map and overall architecture of the Alpine orogen. *Eclogae Geologicae Helvetiae*, *97*(1), 93–117. https://doi.org/10.1007/s00015-004-1113-x

Schmid, S. M., Pfiffner, O. A., Froitzheim, N., Schönborn, G., & Kissling, E. (1996). Geophysical-geological transect and tectonic evolution of the Swiss-Italian Alps. *Tectonics, 15*(5), 1036–1064. https://doi.org/10.1029/96tc00433

Schoene, B., & Bowring, S. A. (2006). U–Pb systematics of the McClure Mountain syenite: thermochronological constraints on the age of the $^{40}Ar/^{39}Ar$ standard MMhb. *Contributions to Mineralogy and Petrology, 151*, 615. https://doi.org/10.1007/s00410-006-0077-4.

Stampfli, G. M., Mosar, J., Marquer, D., Marchant, R., Baudin, T., & Borel, G. (1998). Subduction and obduction processes in the Swiss Alps. *Tectonophysics, 296*(1-2), 159-204.

Steck, A. (1984). Structures et d´eformations tertiaires dans les Alpes centrales. *Eclogae Geologicae Helvetiae*, *77*, 55–100.

Steck, A., Della Torre, F., Keller, F., Pfeifer, H. R., Hunziker, J., & Masson, H. (2013). Tectonics of the Lepontine Alps: Ductile thrusting and folding in the deepest tectonic levels of the Central Alps. *Swiss Journal of Geosciences*, 106(3), 427–450. https://doi.org/10.1007/s00015-013-0135-7.

Steck, A., Epard, J. L., & Masson, H. (2019). The Maggia nappe: an extruding sheath fold basement nappe in the Lepontine gneiss dome of the Central Alps. *International Journal of Earth Sciences, 108,* 2429-2442.

Steiger, R., & Jäger, E. (1977). Subcommission on geochronology: convention on the use of decay constants in geo-and cosmochronology. *Earth and Planetary Science Letters, 36*, 359–362.

Tagliaferri, A., Schenker, F. L., Ulianov, A., Maino, M., & Schmalholz, S. M. (2023). Implications of new geological mapping and U-Pb zircon dating for the Barrovian tectono-metamorphic evolution of the Lepontine dome (Central European Alps). *Geochemistry, Geophysics, Geosystems, 24*(3), e2022GC010772, https://doi.org/10.1029/2022GC010772.

Todd, C. S., & Engi, M. (1997). Metamorphic field gradients in the Central Alps *Journal of Metamorphic Geology, 15*(4), 513–530. https://doi.org/10.1111/j.1525-1314.1997.00038.x.

Trommsdorff, V. (1990). Metamorphism and tectonics in the Central Alps: the Alpine lithospheric mélange of Cima Lunga and Adula. *Memorie della Società Geologica Italiana, 45*, 39–49.

Tumiati, S., Zanchetta, S., Pellegrino, L., Ferrario, C., Casartelli, S., & Malaspina, N. (2018). Granulite-facies overprint in garnet peridotites and kyanite eclogites of Monte Duria (Central Alps, Italy): Clues from srilankite- and sapphirine-bearing symplectites. *Journal of Petrology,* 59(1), 115–152. https://doi.org/10.1093/petrology/egy021.

Vannucchi, P., Sage, F., Morgan, J. P., Remitti, F., & Collot, J.-Y. (2012). Toward a dynamic concept of the subduction channel at erosive convergent margins with implications for

interplate material transfer, *Geochemistry, Geophysics, Geosystems, 13*, Q02003, https://doi.org/10.1029/2011GC003846.

Villa, I. M., Bucher, S., Bousquet, R., Kleinhanns, I. C., & Schmid, S. M. (2014). Dating polygenetic metamorphic assemblages along a transect across the Western Alps. *Journal of Petrology, 55*, 803–830. https://doi.org/10.1093/petrology/egu007.

von Blackenburg, F. (1992). Combined high-precision chronometry and geochemical tracing using accessory minerals: applied to the Central-Alpine Bergell intrusion (central Europe). *Chemical Geology, 100*(1-2), 19-40.

White, R. W., & Powell, R. (2002). Melt loss and the preservation of granulite facies mineral assemblages. *Journal of Metamorphic Geology, 20*, 621-632.

White, R. W., Powell, R., Holland, T. J. B., Johnson, T. E., & Green, E. C. R. (2014). New mineral activity-composition relations for thermodynamic calculations in metapelitic systems. *Journal of Metamorphic Geology, 32*, 261–286.

Whitney, D. L., & Evans, B. W. (2010). Abbreviations for names of rock-forming minerals. *American Mineralogist, 95*, 185–187.

Wiederkehr, M., Bousquet, R., Schmid, S. M., & Berger, A. (2008). From subduction to collision: Thermal overprint of HP/LT meta-sediments in the north-eastern Lepontine Dome (Swiss Alps) and consequances regarding the tectono-metamorphic evolution of the Alpine orogenic wedge. *Swiss Journal of Geosciences*, *101*(1), 127–155. https://doi.org/10.1007/s00015-008-1289-6.

Wiederkehr, M., Sudo, M., Bousquet, R., Berger, A., & Schmid, S. M. (2009). Alpine orogenic evolution from subduction to collisional thermal overprint: The $^{40}Ar/^{39}Ar$ age constraints from the Valaisan Ocean, central Alps. *Tectonics, 28*(6).

Wolff, R., Hölzer, K., Hetzel, R., Dunkl, I., & Anczkiewicz, A. A. (2024). Late-orogenic extension ceases with waning plate convergence: The case of the Simplon normal fault (Swiss Alps). *Journal of Structural Geology, 179*, 105049, https://doi.org/10.1016/j.jsg.2024.105049.

Xiang, H., & Connolly, J. A. (2022). GeoPS: An interactive visual computing tool for thermodynamic modelling of phase equilibria. *Journal of Metamorphic Geology, 40*(2), 243-255.